Journal of Solid Mechanics Vol. 16, No. 3 (2024) pp. 268-287
DOI: 10.60664/jsm.2024.1107148

Research Paper

A Three-Dimensional Deformation Model For Asymmetric Sheet Rolling Process

H. Rezaie, H. Haghighat *

Mechanical Engineering Department, Razi University, Kermanshah, Iran

Received 16 April 2024; Received in revised form 19 September 2024; Accepted 12 October 2024

ABSTRACT

In this paper, a three-dimensional deformation model for analyses of asymmetric sheet rolling process is proposed. The slab method of analysis is used for extracting the rolling parameters diagrams. The sheet material between the upper and the lower rolls is divided into two deformation zones, i.e. entry and exit zones. The entry and exit zones are separated from each other by the plane that connects the upper and lower neutral lines. The intersection line of this plane with the vertical plane which passes through the first contact lines of the sheet with the rolls is found, and the origin of the cylindrical coordinate system is located at the midpoint of it. The mathematical equations of the boundaries of the two deformation zones in the vertical plane of symmetry are defined in the cylindrical coordinate system. The mathematical equation presented to estimate the final width of the sheet in the symmetric rolling is used for asymmetric rolling of the sheet by replacing the equivalent roll radius. It is assumed that the changes in the sheet width in the deformation zone are a linear function of the horizontal distance to the origin. The governing equations on the slabs are derived and the roll force, the roll torque, and the width spread of the sheet are calculated. The theoretical predictions are compared with the FE simulation results obtained by DEFORM 3D ver11. It is found that the predicted loads and width spread of the metal sheet are in good agreement with the FE simulation results.

Keywords: Three-dimensional asymmetric rolling; Slab method of analysis; Width spread; Rolling torque; Rolling force.

1 INTRODUCTION

IN the asymmetrical sheet rolling process, the radius and peripheral velocity of the upper roll can be different from those of the lower roll. It offers benefits such as lower rolling pressure, lower rolling force, and better properties

*Corresponding author. Tel.: +98 83 34274542, Fax: +98 83 34274530.
E-mail address: hhaghighat@razi.ac.ir (H. Haghighat)

.

JOURNAL OF SOLID MECHANICS JSM

of the sheet surface compared to those obtained by conventional symmetrical rolling [1]. In this process, when the initial width-to-thickness ratio of the sheet is less than 10, the width spread cannot be ignored [2]. Therefore, the rolling process is considered as a three-dimensional forming process. Many researchers have analyzed the asymmetric rolling process in two-dimensional, plane strain, and three-dimensional conditions.

Hwang and Tzou [3] analyzed the plane strain asymmetric rolling process experimentally and analytically by using the slab method. In their analysis, they assumed constant shear friction between the sheet and the rolls. Lin and Huang [4] investigated the three-dimensional hot symmetric rolling of sandwich sheets under the assumption of an elastic roller. Hsiang and Lin [5] presented a complex model using the 3D FEM-slab method to save CPU time. The proposed model was a combination of the FE method and the slab method. Compared to traditional FEM, the results of this complex model were acceptable and the proposed model was known as an effective method. Salimi and Sassani [6] analyzed the asymmetric sheet rolling process with the slab method under plane strain conditions. They divided the sheet material between the two rolls into the three deformation zones, i.e. the entry zone, the shear zone, and the outlet zone. Rigid plastic material was considered and the torque and rolling force were estimated.

Komori [7] analyzed the three-dimensional symmetric rolling process of the bar using the upper-bound method. He investigated the effects of reducing the thickness, and the radii of the rolls on the width spread, rolling torque, and rolling force. Salimi and Kodkhodaei [8] investigated the rolling characteristics for a specific condition and concluded that only under certain conditions. They performed their analysis under plane strain conditions. Richelsen and Tvergaard [9] analyzed the three-dimensional cold rolling process to investigate the effect of width spread during rolling. In addition, the effect of different values of the plate width and the roll radius was investigated. In their proposed model, the friction forces in the rolling direction and the transverse direction were calculated. Zhao et al. [10] analyzed the symmetric sheet rolling process using a three-dimensional velocity field. Sezek et al. [11] modeled the three-dimensional symmetric sheet rolling process. They obtained the sheet width by using the upper bound method and presenting a new three-dimensional velocity field using a dual stream function. Gudur et al. [12] estimated the friction coefficient in the plane strain asymmetric rolling process by calculating the curvature of the output sheet. In their analysis, they used the slab method and divided the sheet material between the two rolls into three deformation zones.

Kim et al. [13] proposed an accurate model to obtain the rolling force, and tension distributions in the symmetric rolling process for three-dimensional deformation. They considered the effect of sheet pre-deformation in their model. The effect of pre-deformation of the sheet occurs before the sheet enters the deformation zone, i.e. near the roll entrance. The exact results of the proposed model compared with the predictions of the three-dimensional finite element simulations. An analytical method was proposed by [14] to investigate the rolling torque and rolling force required for the asymmetric sheet rolling process based on the slab method under plane strain conditions. In the analysis, the area between the two rolls was divided into three deformation zones. Hallberg [15] investigated the effect of various parameters such as thickness reduction, friction, and rolling asymmetry factors on grain refinement in the aluminum sheet through numerical simulations. Chen et al. [16] presented a strip layer method to analyze the three-dimensional deformations and stresses of the large cylindrical shell rolling process. They investigated asymmetric factors including the unequal radius and speed of the upper and lower rolls. The obtained results of their method were in good agreement with FEM and experimental results. Zhang et al. [17] analyzed the symmetric sheet rolling process by presenting a three-dimensional velocity field by global weighted method. By calculating the total power functional and minimizing it, the rolling torque, the rolling force, and the stress effective factor are obtained. Comparing the results of the analysis with the experimental results shows a good agreement and the error percentage between them was less than 15.5%. Wu et al. [18] presented a new method to investigate a three-dimensional model of the strip rolling process. They defined an equivalent interfacial layer to integrate the lubrication effect with surface asperity deformation. Liu et al. [19] used a new velocity field and presented the strain rate field to obtain rolling torque and rolling force in a 3D symmetric sheet rolling process. They investigated different rolling conditions such as thickness reduction, friction coefficient on neutral point location, rolling torque, and rolling force. Parvizi and Afrouz [20] analyzed the asymmetric rolling process for pre-bonded clad sheets based on the slab method and FE simulation by the ABAQUS software under plane strain conditions. They assumed non-uniform shear stress and uniform normal stress on the slabs and obtained the torque, rolling force, and the location of the neutral points. Parvizi et al. [21] analyzed the wire rolling process to calculate rolling pressure, rolling force, and rolling torque based on the slab method. In their analysis, they assumed the linear distribution of normal and shear stresses in the vertical sides of the slab. In the proposed model, asymmetric factors such as the inequality of the radius of the rolls, their peripheral velocities, and surface frictions have been investigated. By comparing the analytical results with the FEM simulation data, they achieved a good agreement and showed that by using the analytical solution, the cost and time of computer calculation can be saved. Wang et al. [1] investigated the rolling force, the rolling torque, and the distribution of the pressure under plane strain conditions by using the slab method.

They proposed the optimal pressure state by simultaneously combining different asymmetric conditions that lead to differences in the speeds of the two rolls. They divided the sheet material between the two rolls into three deformation zones, similar to previous researchers. Yao et al. [22] presented a model to predict the distributions of lateral metal flow, tension, and rolling pressure in high-speed hot strip rolling. A quasi-3D approximation is made that preserves the fundamental physics of the problem. The validity of the model was confirmed by comparing the results obtained with the simulation with an error of less than 15%. Sun et al. [23] investigated the asymmetric sheet rolling process with the slab method under plane strain conditions. They divided the area between the two rolls into three deformation zones. Sun et al. [24] analyzed asymmetric rolling by using two analytical models under plane strain conditions. In their analysis, they obtained the rolling torque and force as well as the critical speed ratio of the rolls. Lv et al. [25] analyzed the asymmetric rolling process to investigate the curvature of the output sheet with the experimental method.

Wang and Liu [26] presented an analytical model using the slab method to calculate the minimum rollable thickness in asymmetrical rolling under plane strain conditions. The rolling pressure and force, critical roll speed ratio, and front critical tension were calculated. In their model, four deformation zone configurations were considered. Jiang et al. [27] presented a new model for predicting the exit sheet curvature using the upper bound method, which contradicts the assumption of uniform shear stress in the previous models. They compared the analytical results with experimental and simulation results to demonstrate the validity of their model. Attanasio et al. [28] investigated the sheet rolling process to calculate the pressure distribution on the rolls, force, and torque of the process. In addition, they presented a relationship between the shear friction coefficient and the Coulomb friction coefficient in the rolling process. The authors of this paper proposed a new deformation model for the slab analysis of the plane strain asymmetric sheet rolling process [29]. In the analysis, the sheet material between the upper and the lower rolls was divided into two deformation zones and the rolling parameters diagrams were extracted.

In this paper, the proposed deformation model of [29], is extended to analysis of the three-dimensional asymmetric sheet rolling. The governing equations on the three-dimensional slabs are derived in the cylindrical coordinate system. In the analysis, the effects of thickness reduction, the ratio of the initial width to the initial thickness of the sheet, and the roll radius ratio on the rolling force, rolling torque, as well as the width spread of the sheet are investigated. The calculated rolling force, rolling torque, and sheet width spread are compared with the results obtained from the finite element method.

2 THEORETICAL ANALYSIS

2.1 Geometric relations

The schematic diagram of a three-dimensional asymmetric sheet rolling is shown in Fig. 1. In this process, the sheet with the initial width w_i and the thickness t_i enters the space between the two rolls and during plastic deformation comes out with the final dimensions of width w_f and thickness t_f. The radii of the upper and lower rolls are indicated by R_u and R_l, respectively. According to Fig. 1(a), the upper and lower neutral lines are indicated by $N_{u1}N_{u2}$ and $N_{l1}N_{l2}$, respectively. In the proposed deformation model, similar to the plane strain asymmetric rolling [29], the sheet material between the upper and the lower rolls is divided into two plastic deformation zones, i.e. entry and exit zones. The entry and exit zones are separated from each other by the plane that connects the upper and lower neutral lines, i.e. neutral plane. The mathematical equations of the boundaries of the two deformation zones are defined in the cylindrical coordinate system. The origin of the cylindrical coordinate system, indicated by O in Fig. 1a, is located at the intersection of the neutral plane, and the vertical plane that passes through the first contact lines of the sheet with the rolls. The cross-sectional view in the plane of symmetry of the rolling process is shown in Fig. 1b. In this plane of symmetry, the angles α_{uN}, and α_{lN} denote the angles between the lines C_uN_u and C_lN_l with the vertical plane that connects the centers of the rolls, respectively. The angle θ_N is the angular position of the neutral plane and can be given by

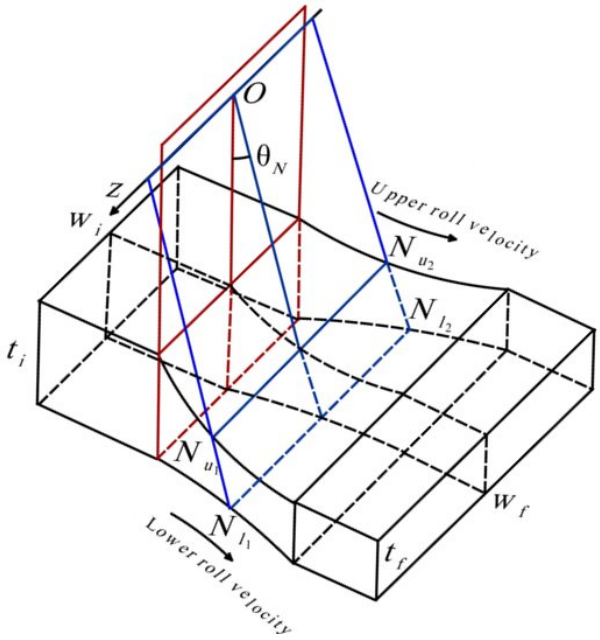

(a)

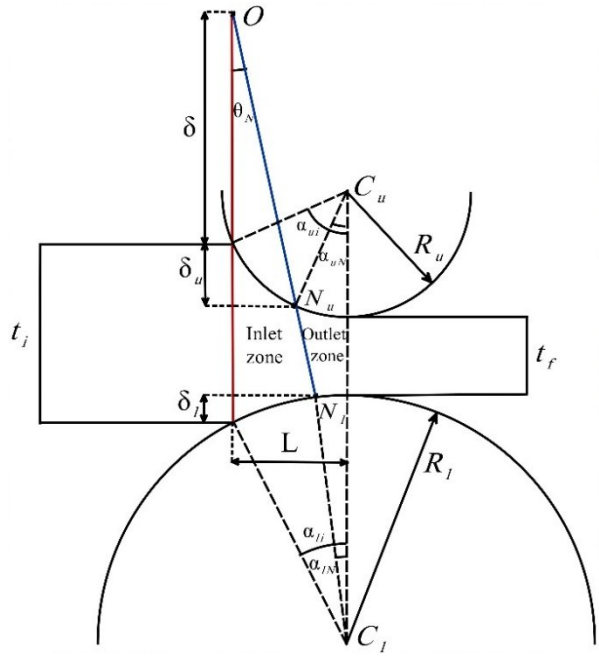

(b)

Fig. 1
Three-dimensional asymmetric sheet rolling, deformation zones, and geometric parameters. (a) The three-dimensional scheme, and (b) Cross-sectional view in the plane of symmetry.

$$\tan\theta_N = \frac{R_u \sin\alpha_{uN} - R_l \sin\alpha_{lN}}{R_u + t_f + R_l - R_u \cos\alpha_{uN} - R_l \cos\alpha_{lN}} \tag{1}$$

The parameter L is the horizontal contact length of the sheet with the rolls and from Fig. 1b can be defined as

$$L = \frac{\sqrt{(t_i - t_f)(2R_u - (t_i - t_f))(2R_l - (t_i - t_f))\left[2(R_u + R_l) - (t_i - t_f)\right]}}{2(R_u + R_l - (t_i - t_f))} \tag{2}$$

Parameter δ is the distance between the origin of the cylindrical coordinate system with the sheet surface and it can be expressed as

$$\delta = \frac{L - R_u \sin\alpha_{uN}}{\tan\theta_N} - \delta_u \tag{3}$$

The geometric parameters δ_u and δ_l shown in Fig. 1b are given by

$$\delta_u = R_u(\cos\alpha_{uN} - \cos\alpha_{ui}) \tag{4}$$

$$\delta_l = R_l(1 - \cos\alpha_{li}) \tag{5}$$

where the angles α_{ui} and α_{li} are shown in Fig. 1b.

2.2 Width spread

The mathematical equation presented to estimate the final width of the sheet in symmetrical rolling [30] has been used for asymmetric rolling of the sheet by replacing the equivalent roll radius R_{eq} as

$$w_f - w_i = \frac{t_i - t_f}{6}\sqrt{\frac{R_{eq}}{t_i}} \tag{6}$$

where

$$R_{eq} = \frac{2R_u R_l}{R_u + R_l} \tag{7}$$

It is assumed that the changes in the sheet width in the deformation zone are a linear function of the horizontal distance to the origin. So the width of the sheet in the deformation zone is given by

$$w = \frac{w_f - w_i}{L} r\sin\theta + w_i \tag{8}$$

Substituting Eq. (6) into Eq. (8), the width of the sheet in the deformation zone is obtained as

$$w = \frac{t_i - t_f}{6L}\sqrt{\frac{R_{eq}}{t_i}}r\sin\theta + w_i \tag{9}$$

2.3 Governing equations

The following assumptions and simplifications have been made to obtain the governing equations:
1. The rolls are assumed to be rigid.
2. The sheet is assumed to be horizontal at the entry and exit.
3. The sheet is assumed to be rigid plastic material and the Tresca yield criterion is used.
4. The friction in the Z direction has been neglected, similar to [17].
The present analysis is based on the slab method. In this method, each of the deformation zones is divided into different slabs and the force equilibrium equations and the yield criterion are extracted. By applying the boundary conditions, the characteristics of the process and the value of load required for the process are obtained.

2.3.1 Slab geometric relations

Fig. 2a shows a slab of the material in angular position θ, and Fig. 2b shows the geometric parameters of the slab in the plane of symmetry. The angles α_u, and α_l are obtained in terms of the angle θ , respectively, by

$$\sin\alpha_u + \tan\theta\cos\alpha_u = \frac{L}{R_u} - \tan\theta\left(\frac{\delta}{R_u} - \cos\alpha_{ui}\right) \tag{10}$$

$$\sin\alpha_l - \tan\theta\cos\alpha_l = \frac{L}{R_l} - \tan\theta\left(\frac{\delta + t_i}{R_l} + \cos\alpha_{li}\right) \tag{11}$$

The width of the slab at the top and bottom, w_u and w_l respectively, are obtained as follows

$$w_{u,l} = \frac{t_i - t_f}{6L}\sqrt{\frac{R_{eq}}{t_i}}r_{u,l}\sin\theta + w_i \tag{12}$$

where r_u and r_l are obtained by

$$r_u = \frac{L - R_u\sin\alpha_u}{\sin\theta} \tag{13}$$

$$r_l = \frac{L - R_l\sin\alpha_l}{\sin\theta} \tag{14}$$

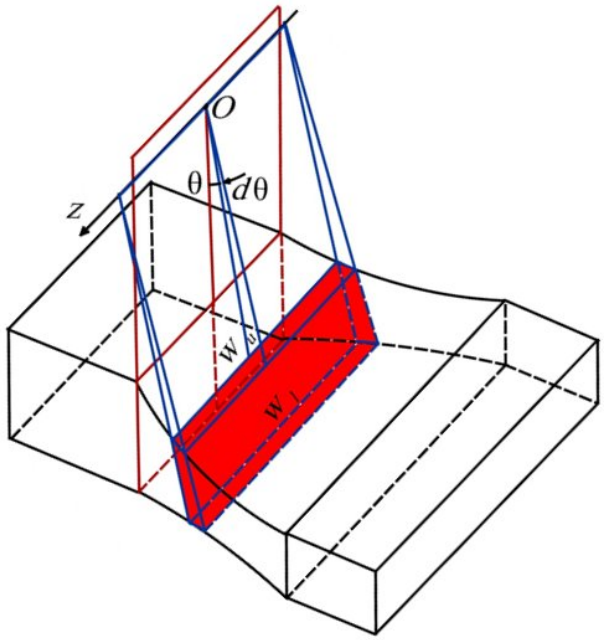

(a)

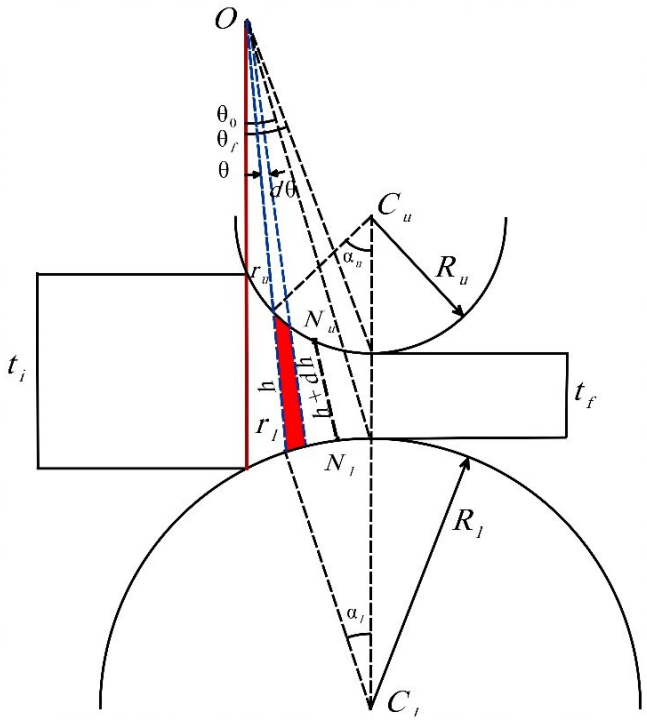

(b)

Fig. 2

A slab of the material in angular position θ, and its geometric parameters

(a) Three-dimensional view, and (b) Cross-sectional view in the plane of symmetry.

The length of the slab in the radial direction, shown by h in Fig. 2b, can be expressed as

$$h = \frac{R_u \sin\alpha_u - R_l \sin\alpha_l}{\sin\theta} \tag{15}$$

In the analysis, the equilibrium equations and the boundary conditions are defined as the functions of the angular position θ .

As indicated in Fig. 2b, the angular positions of the last contact points of the sheet in the plane of symmetry with the lower and upper rolls are indicated by the angles θ_0 and θ_f , respectively and they are given by

$$\tan\theta_0 = \frac{L}{\delta + t_i - \delta_l} \tag{16}$$

$$\tan\theta_f = \frac{L}{\delta + R_u(1-\cos\alpha_{ui})} \tag{17}$$

For the entry zone, the angle θ varies from 0 to θ_N and for the outlet zone, it varies from θ_N to θ_f .

2.3.2 Entry zone $(0 \le \theta \le \theta_N)$

Fig. 3 shows the stresses applied to the slabs in the entry deformation zone. It should be noted that the surface shear stress values are assumed to be constant and are given as $\tau = mk$, where m is the friction factor.

According to Fig. 3, the equilibrium of the radial and circumferential forces acts on the slab in the entry zone, is given by the following equations, respectively.

$$\begin{aligned}&\left[P_u\cos(\alpha_u+\theta)+m_u k\sin(\alpha_u+\theta)\right]w_u\sqrt{r_u^2+(\frac{dr_u}{d\theta})^2}+\frac{\sigma}{2}h(w_u+w_l)+\tau\frac{h}{2}(\frac{dw_u}{d\theta}+\frac{dw_l}{d\theta})-\\&-\left[P_l\cos(\alpha_l-\theta)+m_l k\sin(\alpha_l-\theta)\right]w_l\sqrt{r_l^2+(\frac{dr_l}{d\theta})^2}+\frac{\tau}{2}(w_u+w_l)\frac{dh}{d\theta}+\frac{h}{2}(w_u+w_l)\frac{d\tau}{d\theta}=0\end{aligned} \tag{18}$$

$$\begin{aligned}&\left[-P_u\sin(\alpha_u+\theta)+m_u k\cos(\alpha_u+\theta)\right]w_u\sqrt{r_u^2+(\frac{dr_u}{d\theta})^2}-\frac{h}{2}\sigma(\frac{dw_u}{d\theta}+\frac{dw_l}{d\theta})-\frac{h}{2}(w_u+w_l)\frac{d\sigma}{d\theta}\\&+\left[-P_l\sin(\alpha_l-\theta)+m_l k\cos(\alpha_l-\theta)\right]w_l\sqrt{r_l^2+(\frac{dr_l}{d\theta})^2}-\sigma\frac{(w_u+w_l)}{2}\frac{dh}{d\theta}+\tau h\frac{(w_u+w_l)}{2}=0\end{aligned} \tag{19}$$

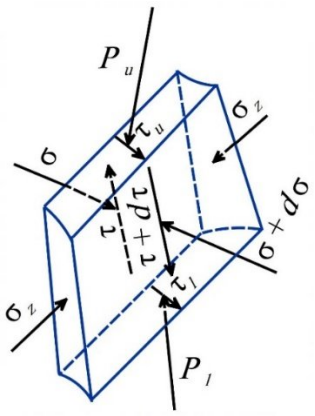

Fig. 3
Stresses applied to the slab in the entry zone.

The yield criterion for the top portion of the slab can be defined as

$$P_u = \sigma - m_u k \tan 2(\alpha_u + \theta) + \frac{2k}{1-\tan^2(\alpha_u+\theta)} \tag{20}$$

For the bottom portion of the slab, the yield criterion can be given by

$$P_l = \sigma - m_l k \tan 2(\alpha_l - \theta) + \frac{2k}{1-\tan^2(\alpha_l-\theta)} \tag{21}$$

By simplifying equilibrium equations and using yield equations, two unknown functions σ and τ are obtained by using two following first-order ordinary differential equations as

$$\begin{aligned}\frac{d\tau}{d\theta} = &-\frac{2w_u}{h(w_u+w_l)}\left[P_u\cos(\alpha_u+\theta)+m_u k\sin(\alpha_u+\theta)\right]\sqrt{r_u^2+\left(\frac{dr_u}{d\theta}\right)^2}-\sigma-\frac{\tau}{h}\frac{dh}{d\theta}+\\ &+\frac{2w_l}{h(w_u+w_l)}\left[P_l\cos(\alpha_l-\theta)+m_l k\sin(\alpha_l-\theta)\right]\sqrt{r_l^2+\left(\frac{dr_l}{d\theta}\right)^2}-\frac{\tau}{w_u+w_l}\left(\frac{dw_u}{d\theta}+\frac{dw_l}{d\theta}\right)\end{aligned} \tag{22}$$

$$\begin{aligned}\frac{d\sigma}{d\theta} = &\frac{2w_u}{h(w_u+w_l)}\left[-P_u\sin(\alpha_u+\theta)+m_u k\cos(\alpha_u+\theta)\right]\sqrt{r_u^2+\left(\frac{dr_u}{d\theta}\right)^2}-\frac{\sigma}{h}\frac{dh}{d\theta}+\tau\\ &+\frac{2w_l}{h(w_u+w_l)}\left[-P_l\sin(\alpha_l-\theta)+m_l k\cos(\alpha_l-\theta)\right]\sqrt{r_l^2+\left(\frac{dr_l}{d\theta}\right)^2}-\frac{\sigma}{w_u+w_l}\left(\frac{dw_u}{d\theta}+\frac{dw_l}{d\theta}\right)\end{aligned} \tag{23}$$

The entrance surface to the entry deformation zone is stress-free, i.e. $\sigma = \tau = 0$, where it is used in solving the differential equations (22) and (23).

2.3.3 Exit zone $(\theta_N \le \theta \le \theta_f)$

Fig. 4 shows the stresses applied to the slab of the sheet material in the exit deformation zone. The equilibrium equations of the forces acting on the slab in radial and circumferential directions for the outlet zone can be written as, respectively

$$\begin{aligned}&\left[P_u \cos(\alpha_u+\theta)-m_u k \sin(\alpha_u+\theta)\right]w_u\sqrt{r_u^2+(\frac{dr_u}{d\theta})^2}+\frac{\sigma}{2}h(w_u+w_l)+\tau\frac{h}{2}(\frac{dw_u}{d\theta}+\frac{dw_l}{d\theta})-\\&-\left[P_l \cos(\alpha_l-\theta)-m_l k \sin(\alpha_l-\theta)\right]w_l\sqrt{r_l^2+(\frac{dr_l}{d\theta})^2}+\frac{\tau}{2}(w_u+w_l)\frac{dh}{d\theta}+\frac{h}{2}(w_u+w_l)\frac{d\tau}{d\theta}=0\end{aligned} \tag{24}$$

$$\begin{aligned}&\left[-P_u \sin(\alpha_u+\theta)-m_u k \cos(\alpha_u+\theta)\right]w_u\sqrt{r_u^2+(\frac{dr_u}{d\theta})^2}-\frac{h}{2}\sigma(\frac{dw_u}{d\theta}+\frac{dw_l}{d\theta})-\frac{h}{2}(w_u+w_l)\frac{d\sigma}{d\theta}\\&+\left[-P_l \sin(\alpha_l-\theta)-m_l k \cos(\alpha_l-\theta)\right]w_l\sqrt{r_l^2+(\frac{dr_l}{d\theta})^2}-\sigma\frac{(w_u+w_l)}{2}\frac{dh}{d\theta}+\tau h\frac{(w_u+w_l)}{2}=0\end{aligned} \tag{25}$$

The yield criteria for the top and the bottom portions of the slab can be expressed as

$$P_u=\sigma+m_u k \tan 2(\alpha_u+\theta)+\frac{2k}{1-\tan^2(\alpha_u+\theta)} \tag{26}$$

$$P_l=\sigma+m_l k \tan 2(\alpha_l-\theta)+\frac{2k}{1-\tan^2(\alpha_l-\theta)} \tag{27}$$

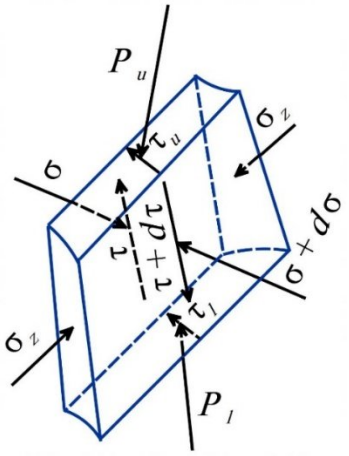

Fig. 4
Stresses applied to the slab of the material in the outlet zone.

By simplifying equilibrium equations and using the yield equations, two unknown functions σ and τ can be obtained by using two first-order ordinary differential equations as

$$\frac{d\tau}{d\theta}=-\frac{2w_u}{h(w_u+w_l)}\left[P_u\cos(\alpha_u+\theta)-m_u k\sin(\alpha_u+\theta)\right]\sqrt{r_u^2+(\frac{dr_u}{d\theta})^2}-\sigma-\frac{\tau}{h}\frac{dh}{d\theta}+$$
$$+\frac{2w_l}{h(w_u+w_l)}\left[P_l\cos(\alpha_l-\theta)-m_l k\sin(\alpha_l-\theta)\right]\sqrt{r_l^2+(\frac{dr_l}{d\theta})^2}-\frac{\tau}{w_u+w_l}(\frac{dw_u}{d\theta}+\frac{dw_l}{d\theta}) \tag{28}$$

$$\frac{d\sigma}{d\theta}=\frac{2w_u}{h(w_u+w_l)}\left[-P_u\sin(\alpha_u+\theta)-m_u k\cos(\alpha_u+\theta)\right]\sqrt{r_u^2+(\frac{dr_u}{d\theta})^2}-\frac{\sigma}{h}\frac{dh}{d\theta}+\tau$$
$$+\frac{2w_l}{h(w_u+w_l)}\left[-P_l\sin(\alpha_l-\theta)-m_l k\cos(\alpha_l-\theta)\right]\sqrt{r_l^2+(\frac{dr_l}{d\theta})^2}-\frac{\sigma}{w_u+w_l}(\frac{dw_u}{d\theta}+\frac{dw_l}{d\theta}) \tag{29}$$

The stress components acting on the sheet material under plastic deformation in the right corner of the outlet zone $(\theta_0\le\theta\le\theta_f)$, are shown in Fig. 5.

The equilibrium equations of the forces acting in the radial and peripheral directions are

$$\left[P_u\cos(\alpha_u+\theta)-m_u k\sin(\alpha_u+\theta)\right]w_u\sqrt{r_u^2+(\frac{dr_u}{d\theta})^2}\,d\theta-\tau h\frac{(w_u+w_l)}{2}=0 \tag{30}$$

$$\left[P_u\sin(\alpha_u+\theta)+m_u k\cos(\alpha_u+\theta)\right]w_u\sqrt{r_u^2+(\frac{dr_u}{d\theta})^2}\,d\theta-\sigma h\frac{(w_u+w_l)}{2}=0 \tag{31}$$

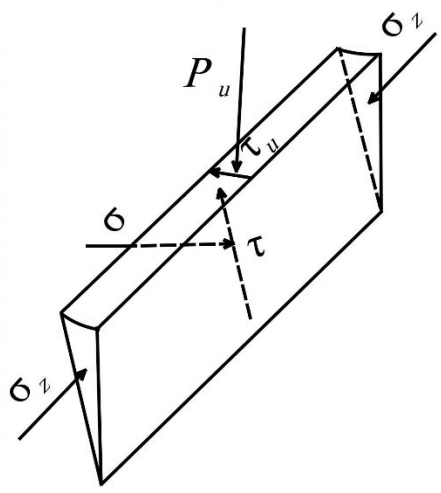

Fig. 5

Stresses acting on the right corner of the exit zone.

By simplifying the equilibrium equations, we have

$$\tau = \frac{2w_u}{h(w_u + w_l)}\left[P_u \cos(\alpha_u + \theta) - m_u k \sin(\alpha_u + \theta)\right]\sqrt{r_u^2 + (\frac{dr_u}{d\theta})^2}\, d\theta \tag{32}$$

$$\sigma = \frac{2w_u}{h(w_u + w_l)}\left[P_u \sin(\alpha_u + \theta) + m_u k \cos(\alpha_u + \theta)\right]\sqrt{r_u^2 + (\frac{dr_u}{d\theta})^2}\, d\theta \tag{33}$$

In the common boundary between the two deformation zones, the neutral plane, the calculated values of σ and τ in the entry and exit zones should be equal.

In summary, the governing equations for the sheet material between the two rolls are given by

$$\begin{aligned}\frac{d\tau}{d\theta} = &-\frac{2w_u}{h(w_u + w_l)}\left[P_u \cos(\alpha_u + \theta) \pm m_u k \sin(\alpha_u + \theta)\right]\sqrt{r_u^2 + (\frac{dr_u}{d\theta})^2} - \sigma - \frac{\tau}{h}\frac{dh}{d\theta} + \\ &+\frac{2w_l}{h(w_u + w_l)}\left[P_l \cos(\alpha_l - \theta) \pm m_l k \sin(\alpha_l - \theta)\right]\sqrt{r_l^2 + (\frac{dr_l}{d\theta})^2} - \frac{\tau}{w_u + w_l}(\frac{dw_u}{d\theta} + \frac{dw_l}{d\theta})\end{aligned} \tag{34}$$

$$\begin{aligned}\frac{d\sigma}{d\theta} = &\frac{2w_u}{h(w_u + w_l)}\left[-P_u \sin(\alpha_u + \theta) \pm m_u k \cos(\alpha_u + \theta)\right]\sqrt{r_u^2 + (\frac{dr_u}{d\theta})^2} - \frac{\sigma}{h}\frac{dh}{d\theta} + \tau \\ &+\frac{2w_l}{h(w_u + w_l)}\left[-P_l \sin(\alpha_l - \theta) \pm m_l k \cos(\alpha_l - \theta)\right]\sqrt{r_l^2 + (\frac{dr_l}{d\theta})^2} - \frac{\sigma}{w_u + w_l}(\frac{dw_u}{d\theta} + \frac{dw_l}{d\theta})\end{aligned} \tag{35}$$

where the upper and lower signs are used for the entry and exit zones, respectively.

2.4 Rolling torque and force

After solving the equilibrium equations of all deformation zones, the upper and lower rolling forces, F_u and F_l respectively, are calculated as follows

$$F_u = \int_0^{\theta_N} w_u \left[P_u \cos\alpha_u + m_u k \sin\alpha_u\right]\sqrt{r_u^2 + (\frac{dr_u}{d\theta})^2}\, d\theta + \int_{\theta_N}^{\theta_f} w_u \left[P_u \cos\alpha_u - m_u k \sin\alpha_u\right]\sqrt{r_u^2 + (\frac{dr_u}{d\theta})^2}\, d\theta \tag{36}$$

$$F_l = \int_0^{\theta_N} w_l \left[P_l \cos\alpha_l + m_l k \sin\alpha_l\right]\sqrt{r_l^2 + (\frac{dr_l}{d\theta})^2}\, d\theta + \int_{\theta_N}^{\theta_0} w_l \left[P_l \cos\alpha_l - m_l k \sin\alpha_l\right]\sqrt{r_l^2 + (\frac{dr_l}{d\theta})^2}\, d\theta \tag{37}$$

The torques of T_u and T_l are the applied torques on the upper and lower rolls, respectively and can be obtained as follows

$$T_u = \int_0^{\theta_N} R_u w_u m_u k \sqrt{r_u^2 + (\frac{dr_u}{d\theta})^2}\, d\theta - \int_{\theta_N}^{\theta_f} R_u w_u m_u k \sqrt{r_u^2 + (\frac{dr_u}{d\theta})^2}\, d\theta \tag{38}$$

$$T_l = \int_0^{\theta_N} R_l w_l m_l k \sqrt{r_l^2 + (\frac{dr_l}{d\theta})^2}\, d\theta - \int_{\theta_N}^{\theta_0} R_l w_l m_l k \sqrt{r_l^2 + (\frac{dr_l}{d\theta})^2}\, d\theta \tag{39}$$

The required rolling torque is expressed as

$$T = T_u + T_l \tag{40}$$

A MATLAB code is developed to solve the governing differential equations in two deformation zones and calculate the required rolling force and rolling torque for the three-dimensional asymmetric rolling process, and for this purpose, the numerical solution used was the Explicit Runge-Kutta method. The inputs of the code include the radii of the rolls, the friction factors between the sheet material and the rolls, the thicknesses of the sheet at the entry and exit, the initial width, and the mean shear yield stress. Finding the necessary torque and rolling force depends on the angular position of the neutral plane θ_N. For a given process conditions, the developed code determines the angular position of the neutral plane θ_N in such a way that the shear and normal stresses, τ and σ, calculated for the neutral plane, from the entry zone be equal to the shear and normal stresses calculated for the neutral plane which are obtained from solving the outlet zone governing equations. Then, knowing the angular position of the neutral plane, the force and rolling torque can be obtained from Eqs. (36-40).

3 FE SIMULATION

To check the validity of the results of the analytical solution for the three-dimensional asymmetric rolling process presented in this paper, the results of the proposed solution are compared with the FE simulation results. DEFORM 3D ver11.0 finite element analysis software is used to simulate the asymmetric rolling process of metal sheets. The finite element mesh used for the simulation of the sheet rolling process for the metal sheet of initial thickness $t_i = 3$ mm and initial width of $w_i = 9$ mm, the upper roll radius of $R_u = 230$ mm, the lower roll radius of $R_l = 250$ mm is shown in Fig. 6. The sheet is modeled as deformable three-dimensional material and meshed with 25000 elements. Using the mesh sensitivity test, the number of elements in the proper deformation volume is checked. The size and number of elements in meshing affect the accuracy of the results, but the results do not change much by increasing the number of elements.

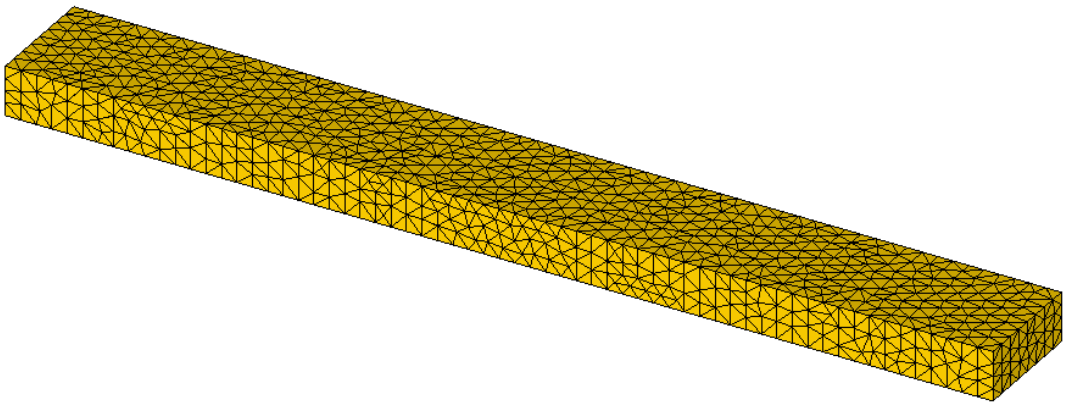

Fig. 6
Initial finite element mesh.

The mechanical properties of the sheet material used in the FE model include the shear yield stress k, modulus of elasticity E, Poisson's ratio v, density of the sheet material and, the constant frictional factor between the material and the rolls where they have been considered as $k = 98.1$ MPa, E =200 GPa, v =0.31, 7800 kg/m^3, and 0.2, respectively. According to the mentioned assumptions, the rolls are modeled as rigid, whereas the metal sheet is assumed a rigid-perfectly plastic material. Furthermore, the upper and lower rolls have the same angular velocities. The angular velocities of the upper and lower rolls are set to be equal to 9.5 rpm. The sheet after deformation and deformed finite element mesh is shown in Fig. 7.

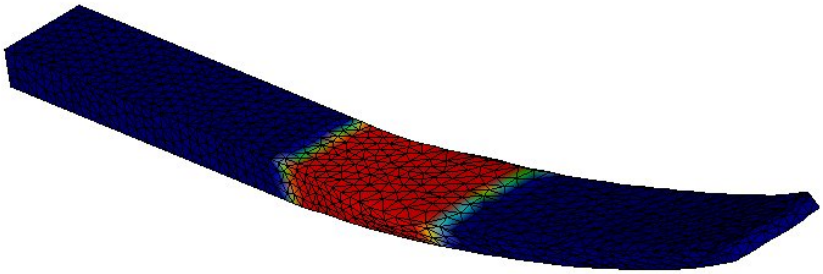

Fig. 7
Deformed mesh.

4 ANALYTICAL RESULTS AND DISCUSSION

The relationship between rolling torque and the roll radius ratio is shown in Fig. 8. According to this figure, geometrical data and mechanical properties are, $t_i = 3$ mm, $w_i = 9$ mm, $R_l = 250$ mm, $m_u = m_l = 0.2$, $k = 98.1$ MPa, $r = 50\%$, where r is the reduction percentage in thickness and is given by

$$r\% = \frac{t_i - t_f}{t_i} \times 100 \tag{41}$$

The rolling torque decreases with an increase in the roll radius ratio as shown in Fig. 8. It is found from Fig. 8 that the required rolling torque in the asymmetric rolling process is smaller than that of symmetric rolling process in which the roll radius ratio is equal to 1. It is also confirmed from Fig. 8 that the rolling torques calculated based on the present model are in good agreement with the FEM results.

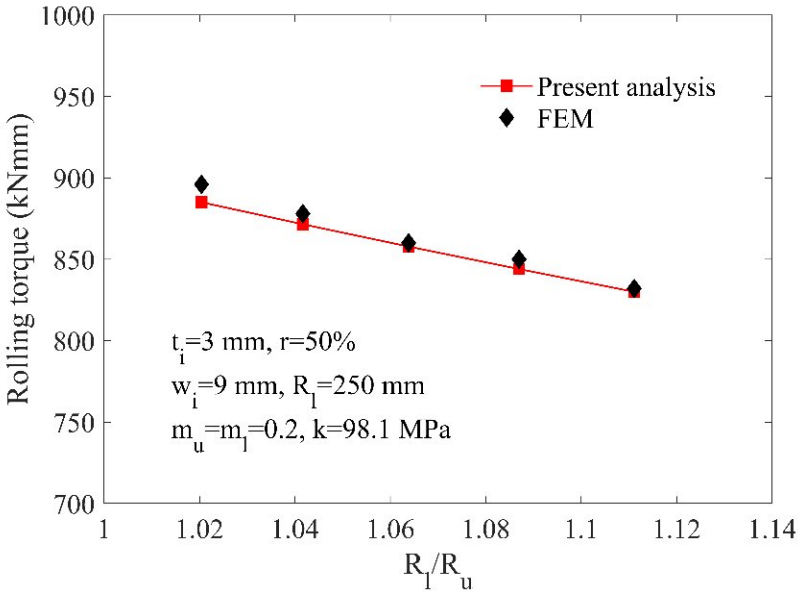

Fig. 8
The relationship between the rolling torque and the roll radius ratio.

Fig. 9 displays the relationship between rolling force and the roll radius ratio. According to this figure, geometrical data and mechanical properties of the sheet material are as shown in Fig. 8, and the results of the present analytical model are also compared with the FE simulation data. From this figure, it can be seen that the rolling force, similar to rolling torque, in the asymmetric rolling process is smaller than that of the symmetric rolling process. It is also confirmed from Fig. 9 that the analytical results are in good agreement with the FE simulation data. From Figs. 8 and 9, it can be seen that the sensitivity of the rolling force is lower than the rolling torque with the roll radius ratio.

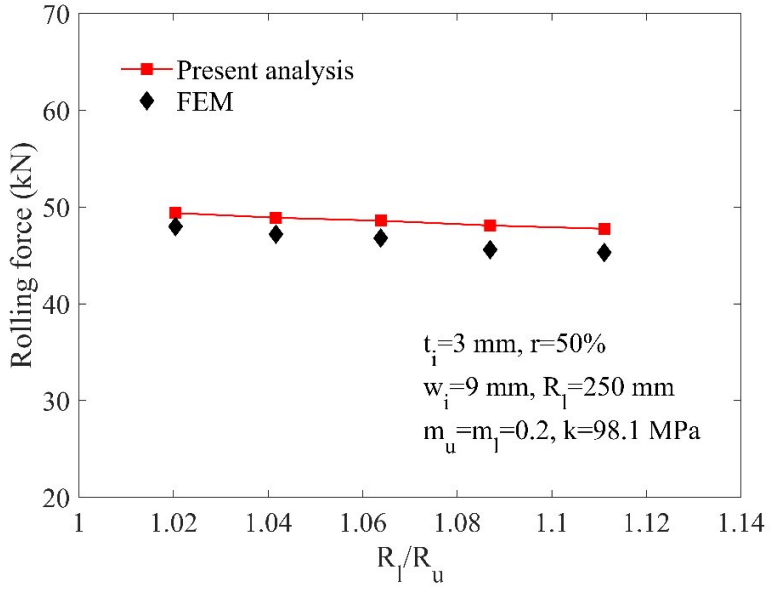

Fig. 9
The relationship between the rolling force and the roll radius ratio.

Fig. 10 shows the effect of the reduction in thickness on the width of the sheet at the exit for the process conditions represented in the figure. According to this figure, the geometrical data and the mechanical properties are, $t_i = 3\,\text{mm}$, $w_i = 9\,\text{mm}$, $R_u = 230\,\text{mm}$, $R_l = 250\,\text{mm}$, $m_u = m_l = 0.35$, $k = 98.1$ MPa. This figure illustrates that the width of the sheet at the exit becomes high with increasing the reduction in thickness value. From this figure, it can be seen that the width of the sheet at the exit is approximately proportional to the reduction in thickness. This figure also displays the comparison between the results obtained from the analysis and the FE simulation data. It can be seen that there is a good agreement between the FE data and the results of the slab method of analysis.

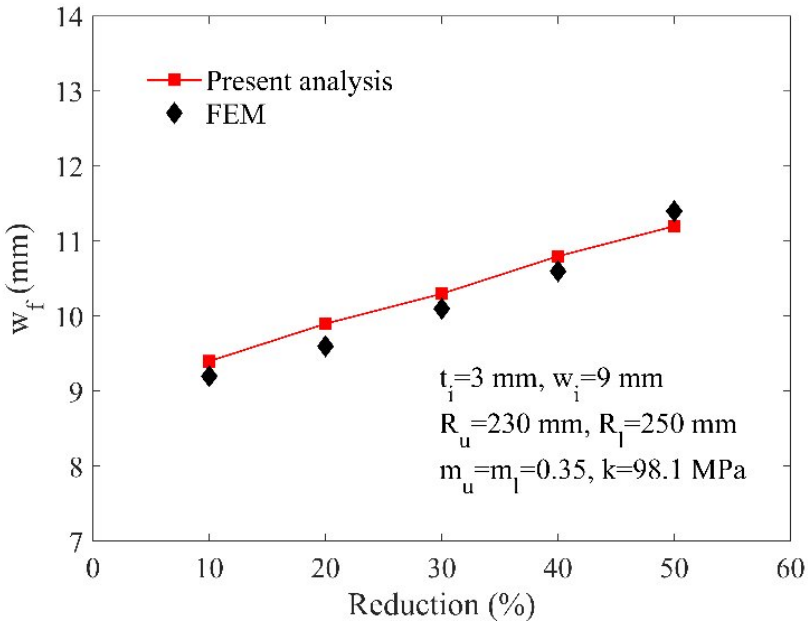

Fig. 10
The effect of the reduction percentage on the width of the output strip.

Fig. 11 illustrates the variation of the ratio of final width to initial width with the ratio of initial width-to-thickness for two different reductions in thickness. It is observed that when the initial width-to-thickness is increased, the ratio of final width to initial width decreases. From this figure, it can be seen that for a given ratio of initial width-to-thickness, the ratio of final width to initial width increases by increasing the reduction in thickness value. For the initial width-to-thickness ratio greater than 15, the output width is approximately equal to the initial width, and the width spread can be ignored. Therefore, it is expected that the ratio of the width at the exit to the initial width of the sheet remains constant and the slope of the diagram is equal to the zero approximately. In this figure, the geometrical data, friction factors and the mechanical properties of the sheet material are, $t_i = 3\,\text{mm}$, $R_u = 230\,\text{mm}$, $R_l = 250\,\text{mm}$, $m_u = m_l = 0.2$, $k = 98.1$ MPa, respectively.

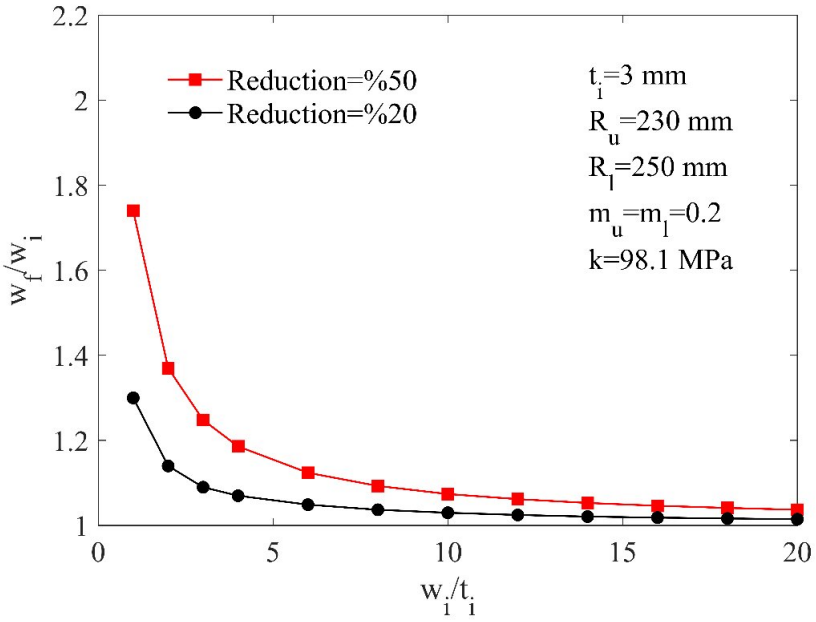

Fig. 11
Variation of the ratio of final width to initial width with the ratio of initial width-to- thickness for two different reductions in thickness.

To further investigate, the three-dimensional results have been compared with plane strain values. Fig. 12 shows the comparison of the three-dimensional rolling force per unit initial width, with plane strain analysis [12], and experiment [3]. It can be seen that in the initial width-to-thickness ratio of less than 15, there is a big difference between the three-dimensional results of the present analysis with the experiment and plane strain results. However, since the initial width-to-thickness ratio becomes greater than 15, the amount of three-dimensional force per unit of initial width is equal to plane strain values and experimental results. In fact, at a constant initial thickness, as the initial width of the sheet increases, the amount of three-dimensional rolling force per initial width is equal to that of plane strain analysis result. According to this figure, geometrical data and mechanical properties are, $t_i = 2\,\text{mm}$, $R_u = 50\,\text{mm}$, $m_u = m_l = 0.272$, $k = 85$ MPa, $r = 48\%$.

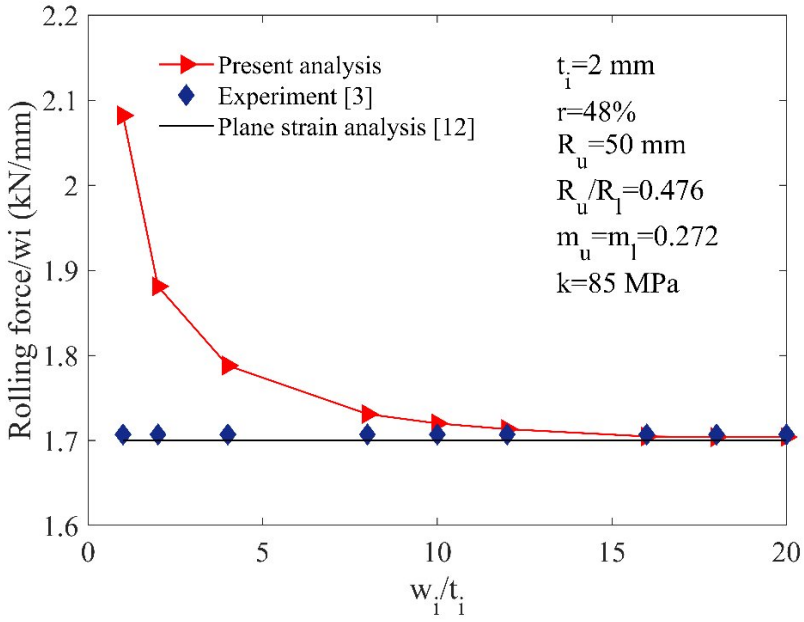

Fig. 12
Comparison of the variation of the rolling force per initial width with the ratio of the initial width-to-thickness for three-dimensional and plane strain analysis.

Fig. 13 comprises the variation of the rolling torque per initial width with the ratio of the initial width-to-thickness for the three-dimensional process and plane strain analysis [14].

This figure shows that as the initial width-to-thickness ratio increases, the rolling torque per initial width increases, but this increase is approximately saturated with the initial width-to-thickness ratio greater than 15. Therefore, for the asymmetric rolling process of a sheet with the initial width-to-thickness ratio greater than 15, the three-dimensional process can be assumed as a two-dimensional process, i.e. a plane strain forming process. According to this figure, geometrical data and mechanical properties are, $t_i = 4\,\text{mm}$, $R_u = 350\,\text{mm}$, $m_u = m_l = 0.35$, $k = 98.1$ MPa, $r = 10\%$.

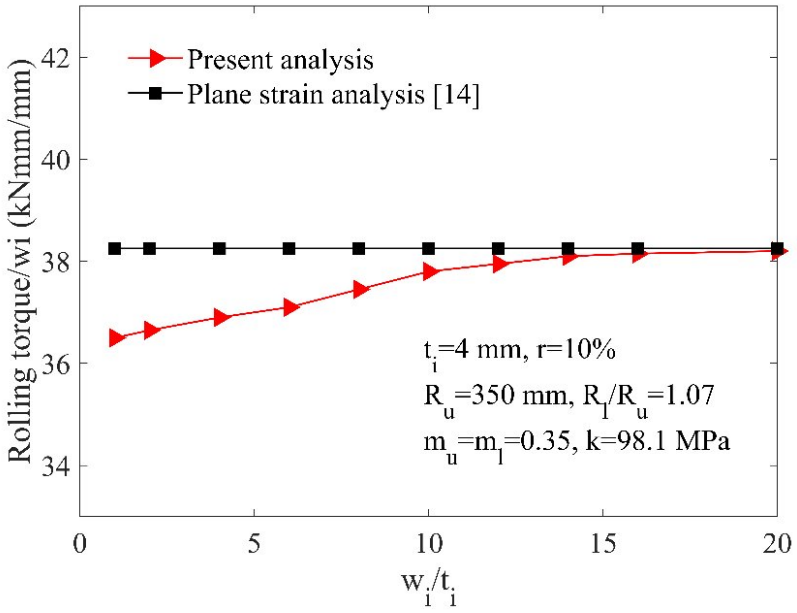

Fig. 13
Comparison of the variation of the rolling torque per initial width with the initial width-to-thickness ratio for the three-dimensional and plane strain analysis.

5 CONCLUSIONS

A mathematical model, based on the slab method of analysis, considering two deformation zones has been proposed to analysis the three-dimensional asymmetric sheet rolling process. To check the validity of this model, the FEM is also used to simulate the three-dimensional forming process. The effects of various process conditions, such as the roll radius ratio, the reduction in thickness, etc., upon the rolling torque, rolling force, and the width of the sheet at the exit have been discussed. The rolling torque, rolling force, and the width of the sheet at the exit are quite coincident with those by the FEM. From the analytical results, it is known that the rolling torque and rolling force decrease with increasing roll radius ratio. The rolling torque per unit of initial width increases and the rolling force per unit of initial width decreases with increasing the initial width-to-thickness ratio. For the asymmetric rolling process of a sheet with an initial width-to-thickness ratio greater than 15, the three-dimensional process can be assumed as a two-dimensional process, i.e. plane strain forming process. In the sheet rolling industry, the calculated rolling torque and rolling force are used to design rolling machine components. It is also used to calculate the required electro motor power capacity.

REFERENCES

[1] Wang J, Liu X, Guo W., 2018, Analysis of mechanical parameters for asymmetrical strip rolling by slab method. Int J Adv Manuf Technol **98**: 2297–2309.
[2] Wang JP, Kao WC, Lee HD, Wang J., 2008, Analysis of 3D rolling forming with generalized rigid-plastic boundaries approach. J Mater Process Technol **204**: 425–433.
[3] Hwang YM, Tzou GY., 1997, Analytical and experimental study on asymmetrical sheet rolling. Int J Mech Sci **39**: 289–303.
[4] Lin ZC, Huang TG., 2000, Different degree of reduction and sliding phenomenon study for three-dimensional hot rolling with sandwich flat strip. Int J Mech Sci **42**: 1983–2012.
[5] Hsiang SH, Lin SL., 2001, Application of 3D FEM-slab method to shape rolling. Int J Mech Sci **43**: 1155–1177. https://doi.org/10.1016/S0020-7403(00)00064-3
[6] Salimi M, Sassani F., 2002, Modified slab analysis of asymmetrical plate rolling. Int J Mech Sci **44**: 1999–2023.
[7] Komori, K., 2002, An upper bound method for analysis of three-dimensional deformation in the flat rolling of bars. Int J Mech Sci **44**: 37–55.
[8] Salimi M, Kadkhodaei M., 2004, Slab analysis of asymmetrical sheet rolling. J Mater Process Technol **150**: 215–222.
[9] Richelsen AB, Tvergaard V., 2004, 3D Analysis of cold rolling using a constitutive model for interface friction. Int J Mech Sci **46**: 653–671.
[10] Zhao DW, Xie YJ, Liu XH, Wang GD., 2006, Three-dimensional analysis of rolling by twin shear stress yield criterion. Journal of Iron and Steel Research International **13**: 21–26.
[11] Sezek S, Aksakal B, Can Y., 2008, Analysis of cold and hot plate rolling using dual stream functions. Materials & Design **29**: 584–596.
[12] Gudur PP, Salunkhe MA, Dixit US. A theoretical study on the application of asymmetric rolling for the estimation of friction. Int J Mech Sci 2008;50: 315–327.
[13] Kim YK, Kwak WJ, Shin TJ., 2010, A new model for the prediction of roll force and tension profiles in flat rolling. ISIJ international **50**: 1644–1652.
[14] Zhang SH, Zhao DW, Gao CR, Wang GD., 2012, Analysis of asymmetrical sheet rolling by slab method. Int J Mech Sci **65**: 168–176.
[15] Hallberg H., 2013, Influence of process parameters on grain refinement in AA1050 aluminum during cold rolling. Int J Mech Sci **66**: 260–272.
[16] Chen SW, Liu HM, Peng Y, Sun, JL., 2013, Strip layer method for simulation of the three-dimensional deformations of large cylindrical shell rolling. Int J Mech Sci **77**: 113–120.
[17] Zhang S, Song B, Wang X, Zhao D., 2014, Analysis of plate rolling by MY criterion and global weighted velocity field. Applied Mathematical Modelling **38**: 3485–3494.
[18] Wu C, Zhang L, Li S, Jiang Z, Qu P., 2014, A novel multi-scale statistical characterization of interface pressure and friction in metal strip rolling. Int J Mech Sci **89**: 391–402.
[19] Liu YM, Ma GS, Zhao DW, Zhang DH., 2015, Analysis of hot strip rolling using exponent velocity field and MY criterion. Int J Mech Sci **98**: 126–131.
[20] Parvizi A, Afrouz F., 2016, Slab analysis of asymmetrical clad sheet bonded before the rolling process. Int J Adv Manuf Technol **87**: 137–150.
[21] Parvizi A, Pasoodeh B, Abrinia K., 2016, An analytical approach to asymmetrical wire rolling process with finite element verification. Int J Adv Manuf Technol **85**: 381–389.
[22] Yao C, He A, Shao J, Zhao J., 2019, A real-time quasi-3D metal flow model for hot strip rolling. Int J Mech Sci **159**: 91–102.
[23] Sun X, Liu X, Wang J, Qi J., 2020, Analysis of asymmetrical rolling of strip considering percentages of three regions in the deformation zone. Int J Adv Manuf Technol **110**: 763–775.
[24] Sun X, Liu X, Wang J, Qi J., 2020, Analysis of asymmetrical rolling of strip considering two deformation region types. Int J Adv Manuf Technol **110**: 2767–2785.
[25] Lv M, Zhang L, He B, Zhao F, Li S, Wang X., 2021, Experimental study on the cross-shear roll bending process. Int J Adv Manuf Technol **115**: 1487–1496.
[26] Wang J, Liu X., 2022, Study on minimum rollable thickness in asymmetrical rolling. Int J Adv Manuf Technol **119**: 2223–2233.
[27] Jiang LY, Liang JL, Chen YF, Shi JH, Ma LF., 2024, The curvature modeling for the double layered clad plate by asymmetric rolling with different diameters. Int J Adv Manuf Technol **131**: 3793–3809.
[28] Attanasio A, Del Prete A, Primo T., 2024, Numerical and analytical estimation of rolling force and torque in hot strip rolling. Int J Adv Manuf Technol **130**: 1855–1869.
[29] Rezaie H, Haghighat, H., 2024, A new deformation model for plane strain asymmetric sheet rolling process. Int J Adv Manuf Technol **134**: 2575-2586.
[30] Lange K, Handbook of metal forming. 1st ed edition, United States of America: Society of manufacturing engineers 1985; 1204.